

Supplementary Material

**Enabling high loading of well-dispersed Ni<sub>2</sub>CoP<sub>2</sub> catalysts on 3D-printed electrode for efficient electrocatalysis**

Meiwen Peng<sup>a</sup>✉, Bo Zhao<sup>a</sup>✉, Danli Shi<sup>a</sup>, Yawen Wang<sup>a</sup>, Dong Li<sup>a</sup>, Wenkai Liang<sup>a</sup>, He Yang<sup>a</sup>, Zhiqiang Liang<sup>a</sup>, Yinghui Sun<sup>b</sup>\*, and Lin Jiang<sup>a</sup>\*

<sup>a</sup>Institute of Functional Nano & Soft Materials Laboratory (FUNSOM), Jiangsu Key Laboratory for Carbon-Based Functional Materials & Devices, Soochow University, Suzhou 215123, China

<sup>b</sup>Innovation Center for Chemical Sciences, College of Chemistry, Chemical Engineering and Materials Science, Soochow University, Suzhou, 215123, China

\*Correspondence and requests for materials should be addressed to Lin Jiang (E-mail: [lijiang@suda.edu.cn](mailto:lijiang@suda.edu.cn)) or to Yinghui Sun (E-mail: [yinghuisun@suda.edu.cn](mailto:yinghuisun@suda.edu.cn))

✉ These authors contributed equally to this work.

## Supplementary Figures

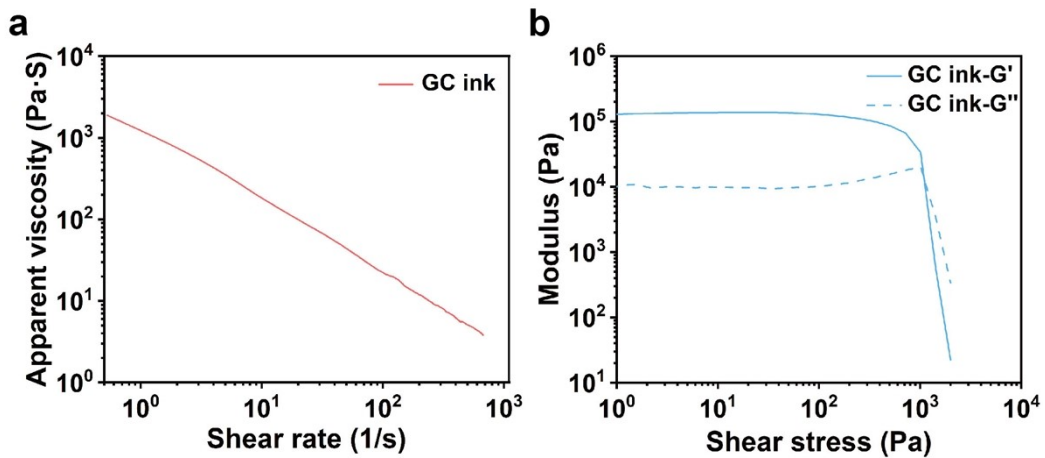


**Fig. S1.** (a) Apparent viscosity as a function of shear rate for GC inks. (b) Storage modulus ( $G'$ ) and loss modulus ( $G''$ ) as a function of shear stress for GC ink.

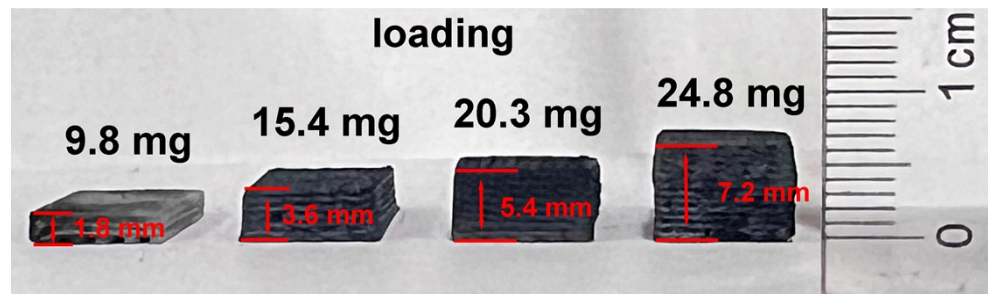


**Fig. S2.** The optical photo of different 3DP GC electrodes with 6, 12, 18, and 24 layers.

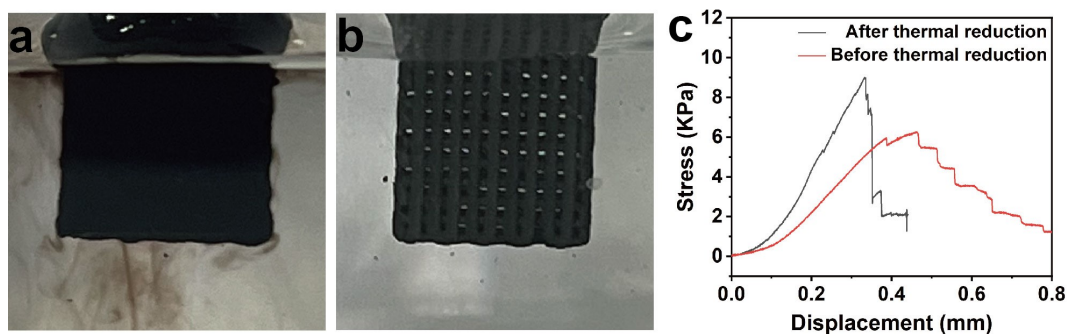


**Fig. S3.** (a) The 3DP GC electrode before thermal reduction, (b) The 3DP GC electrode after thermal reduction, (c) Flexural stress.

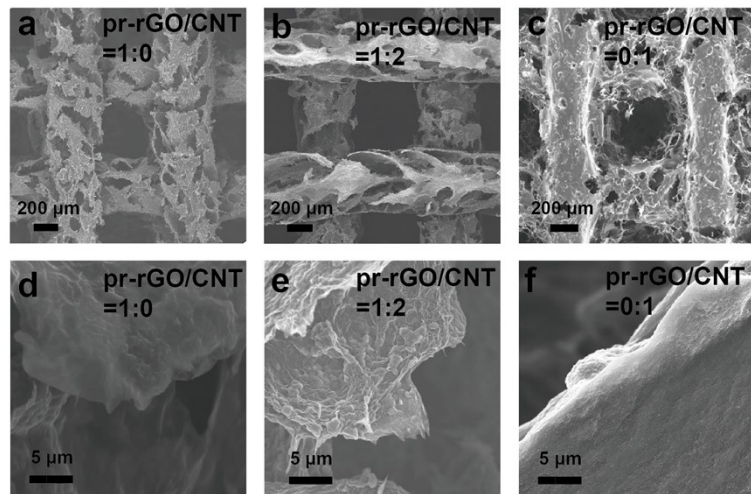


**Fig. S4.** SEM characterization of three electrodes with different GC proportions (a, d) pr-rGO/CNT=1:0, (b, e) pr-rGO/CNT=1:2, (c, f) pr-rGO/CNT=0:1.

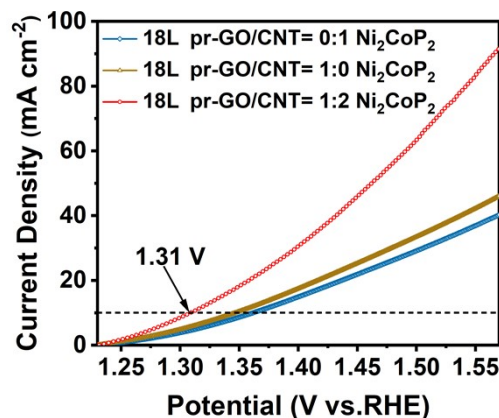


**Fig. S5.** The polarization curves of 18L-3DP electrodes with different ratios of CNT and pr-GO.

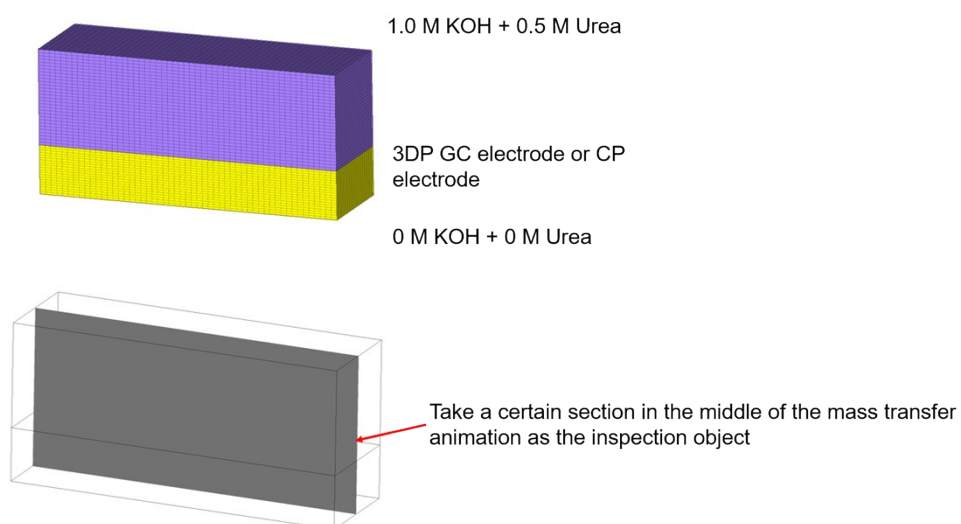


**Fig. S6.** The mass transport model.

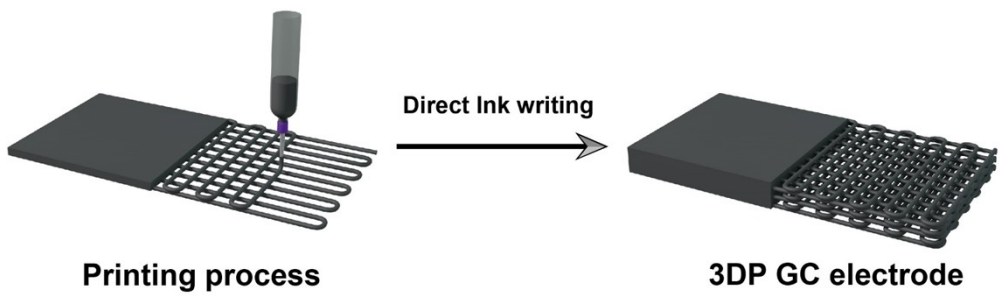


**Fig. S7.** The printing process of 3DP GC

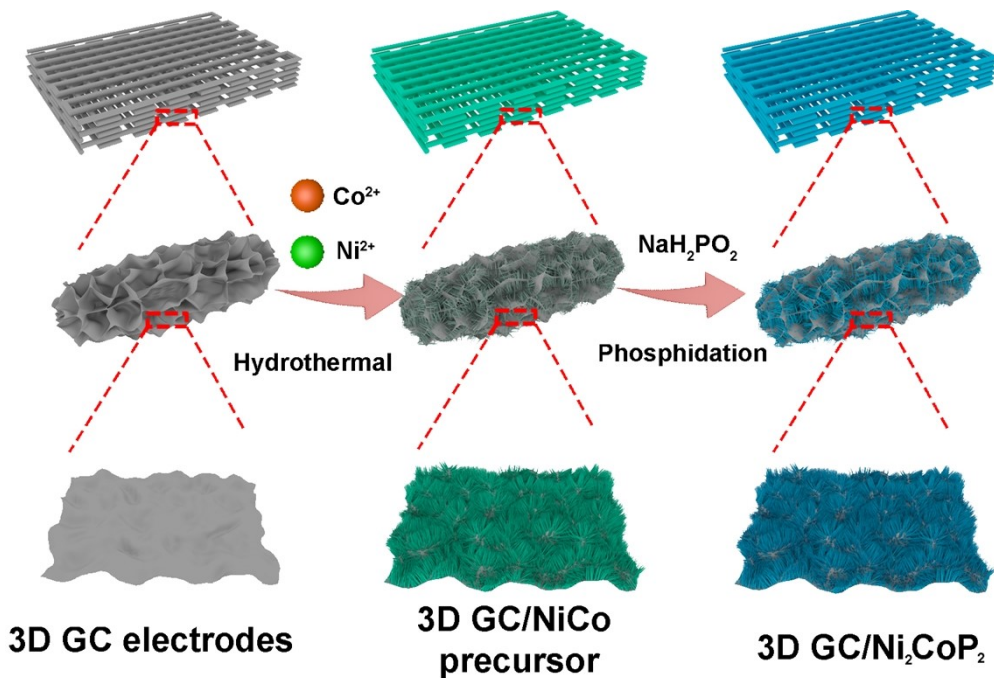


**Fig. S8.** The preparation of 3DP GC/Ni<sub>2</sub>CoP<sub>2</sub>.

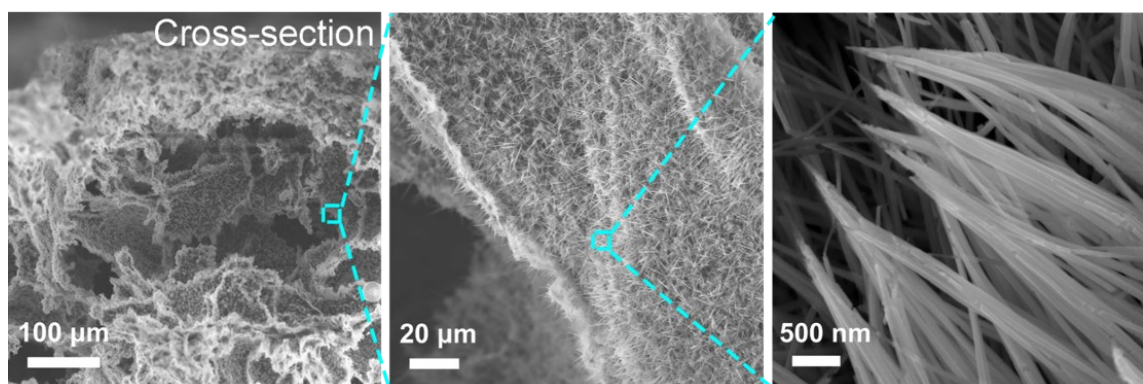


**Fig. S9.** The SEM images of 3DP GC/Ni<sub>2</sub>CoP<sub>2</sub> (cross-section).

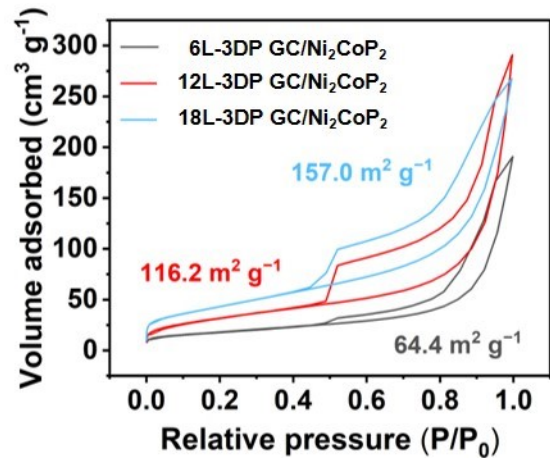


**Fig. S10.** N<sub>2</sub> sorption isotherm of 6L, 12L, 18L-3DP GC/Ni<sub>2</sub>CoP<sub>2</sub>.

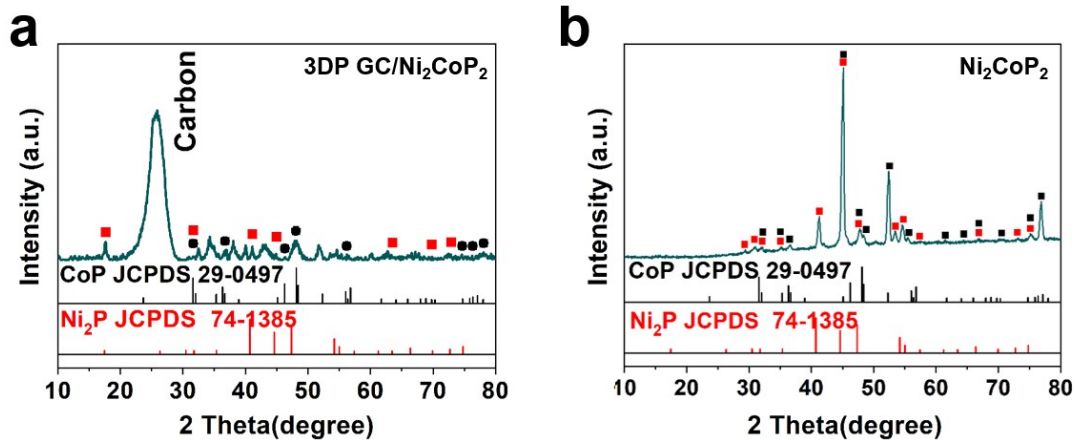


**Fig. S11.** XRD spectrum of a) 3DP GC/Ni<sub>2</sub>CoP<sub>2</sub>, b) Ni<sub>2</sub>CoP<sub>2</sub>. (red square for Ni<sub>2</sub>P, black square for CoP)

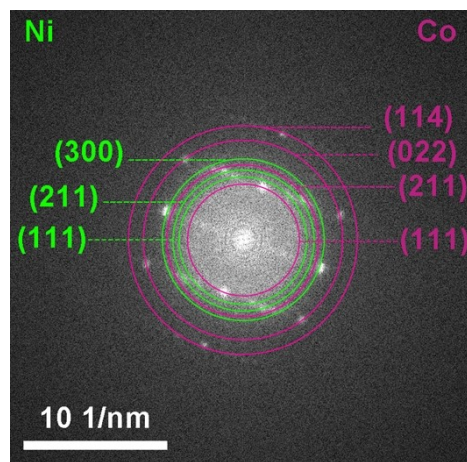


**Fig. S12.** The SAED pattern of Ni<sub>2</sub>CoP<sub>2</sub>.

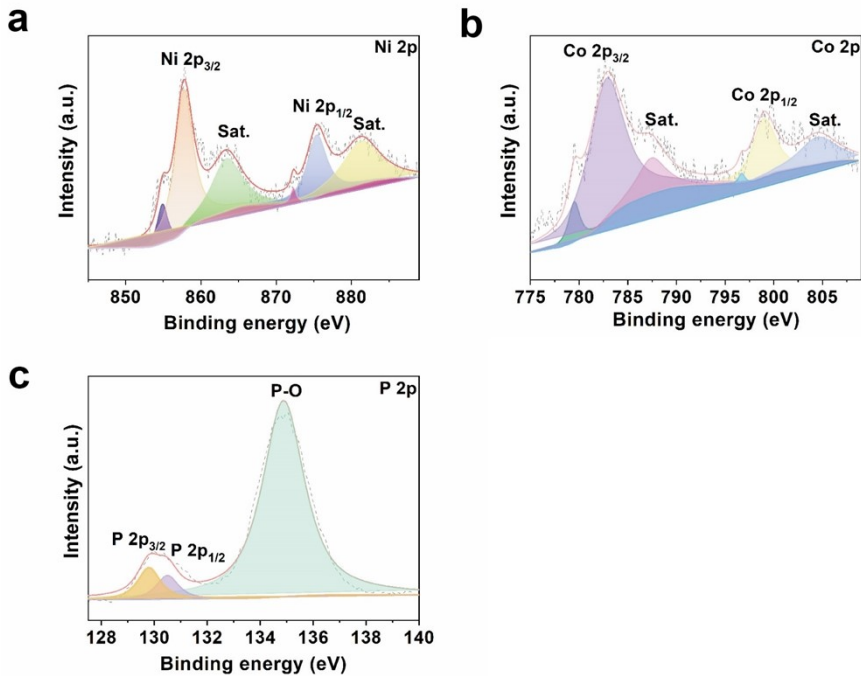


**Fig. S13.** High-resolution XPS spectra of 3DP GC/Ni<sub>2</sub>CoP<sub>2</sub>, a) Ni 2p, b) Co 2p, c) P 2p.

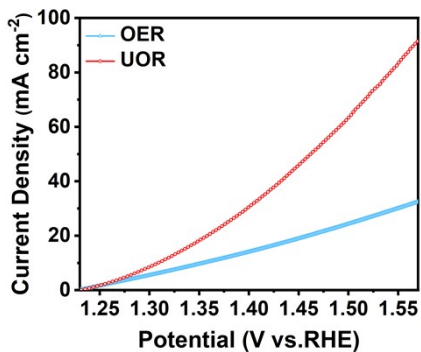


**Fig. S14.** UOR and OER LSV curves of 18L-3DP GC/Ni<sub>2</sub>CoP<sub>2</sub>.

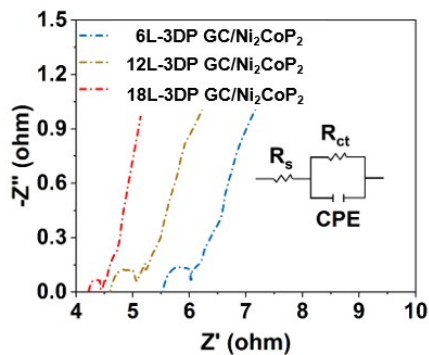


**Fig. S15.** Nyquist plots of different electrocatalysts for UOR.

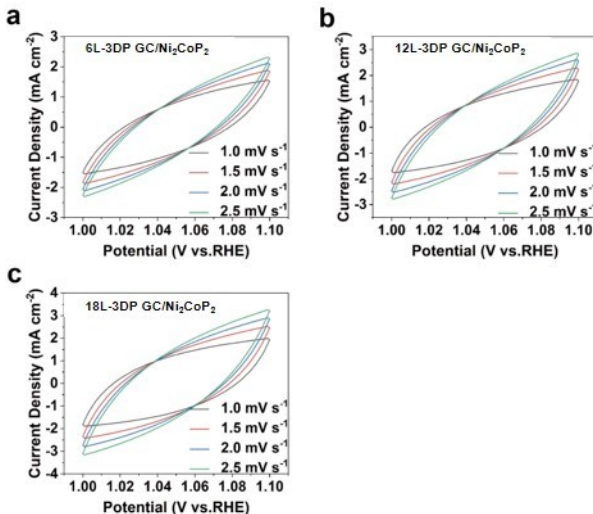


**Fig. S16.** CV curves of 3DP GC/Ni<sub>2</sub>CoP<sub>2</sub> with different layers with different rate from 1 to 2.5 mV s<sup>-1</sup> for UOR.

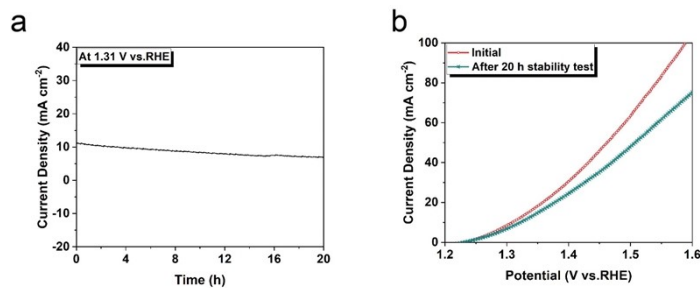


**Fig. S17.** a) Chronopotentiometry plots of 18L-3DP GC/Ni<sub>2</sub>CoP<sub>2</sub> obtained at a constant potential of 1.31 V for UOR. b) LSV curves of 18L-3DP GC/Ni<sub>2</sub>CoP<sub>2</sub> before and after 20 h stability for UOR.

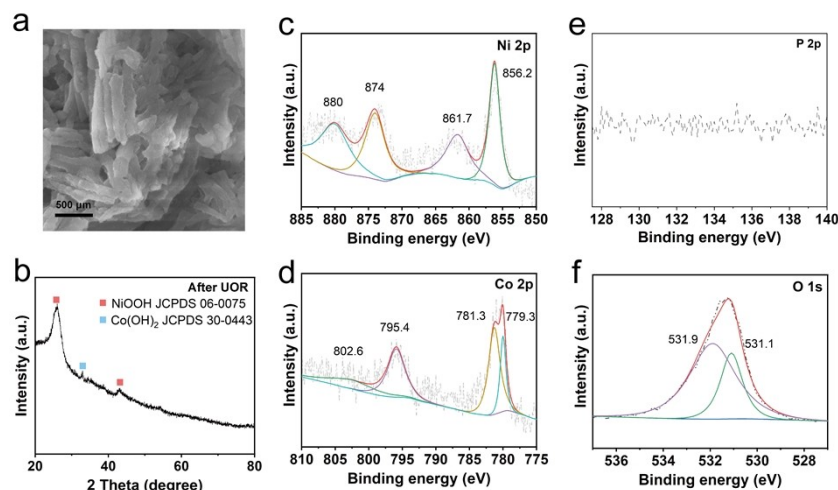


**Fig. S18.** a) The SEM of Ni<sub>2</sub>CoP<sub>2</sub> after UOR, b) The XRD of Ni<sub>2</sub>CoP<sub>2</sub> after UOR, c-f) The XPS of Ni<sub>2</sub>CoP<sub>2</sub> after UOR.

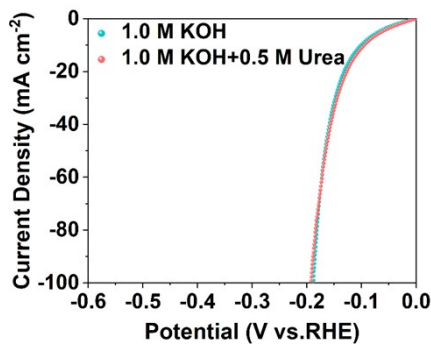


**Fig. S19.** HER LSV curves of 18L-3DP GC/Ni<sub>2</sub>CoP<sub>2</sub> in 1.0 M KOH and 1.0 M KOH with 0.5 M urea.

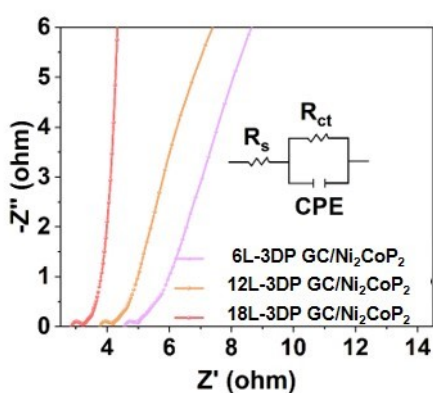


**Fig. S20.** Nyquist plots of different electrocatalysts for the HER.

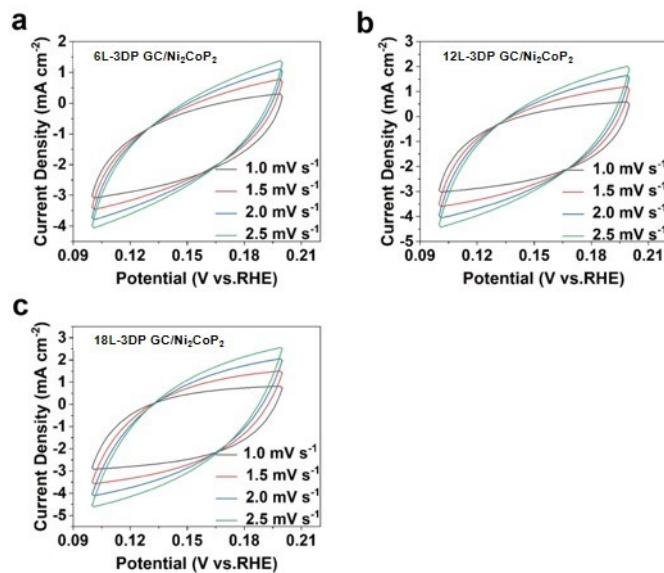


**Fig. S21.** CV curves of 3DP GC/Ni<sub>2</sub>CoP<sub>2</sub> with different layers with different rate from 1 to 2.5 mV s<sup>-1</sup> for HER.

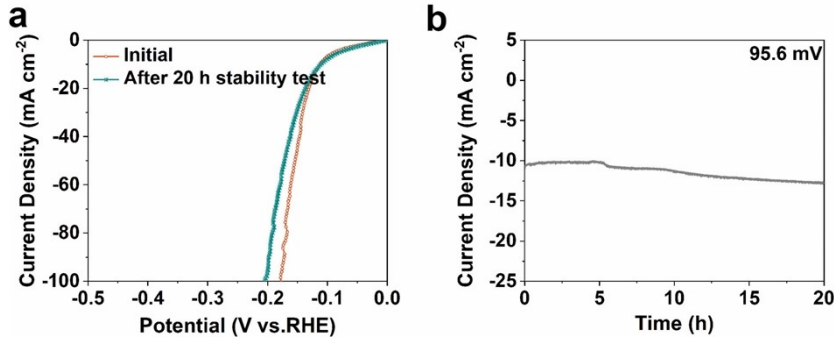


**Fig. S22.** a) LSV curves of 18L-3DP GC/ $\text{Ni}_2\text{CoP}_2$  before and after 20 h stability test for the HER. b) Chronopotentiometry plots of 18L-3DP GC/ $\text{Ni}_2\text{CoP}_2$  obtained at a constant potential of 0.0956 V for HER.

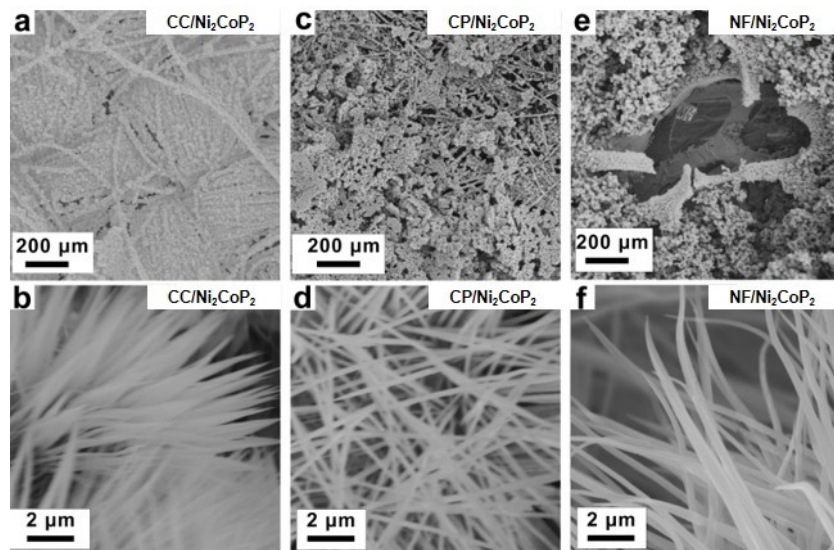


**Fig. S23.** The SEM images of  $\text{Ni}_2\text{CoP}_2$  on (a,b) CC, (c,d) CP, (e,f) NF.

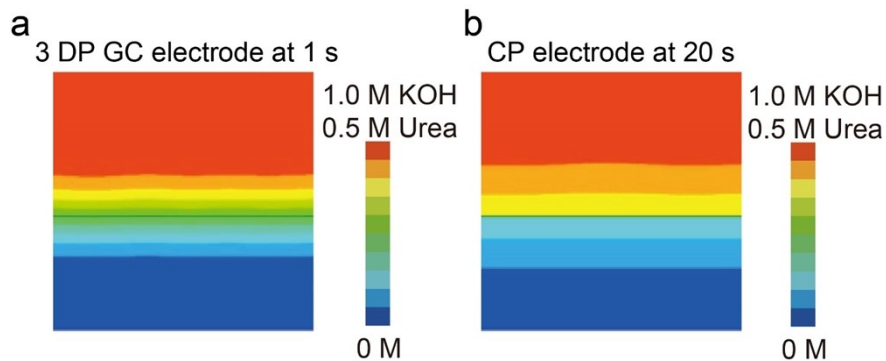


**Fig. S24.** Simulation of 1.0 M KOH + 0.5 M urea mass transfer under different 3D structured electrodes. a) 3DP GC electrode. b) CP electrode.

**Table S1.** The corresponding EIS parameters of the 6L-3DP GC/Ni<sub>2</sub>CoP<sub>2</sub>, 12L-3DP GC/Ni<sub>2</sub>CoP<sub>2</sub> and 18L-3DP GC/Ni<sub>2</sub>CoP<sub>2</sub> for UOR.

	18L-3DP GC/Ni <sub>2</sub> CoP <sub>2</sub>	12L-3DP GC/Ni <sub>2</sub> CoP <sub>2</sub>	6L-3DP GC/Ni <sub>2</sub> CoP <sub>2</sub>
R <sub>s</sub> (Ω cm <sup>2</sup> )	4.22	4.60	5.52
R <sub>ct</sub> (Ω cm <sup>2</sup> )	0.24	0.52	0.59

**Table S2.** The corresponding EIS parameters of the 6L-3DP GC/Ni<sub>2</sub>CoP<sub>2</sub>, 12L-3DP GC/Ni<sub>2</sub>CoP<sub>2</sub> and 18L-3DP GC/Ni<sub>2</sub>CoP<sub>2</sub> for HER.

	18L-3DP GC/Ni <sub>2</sub> CoP <sub>2</sub>	12L-3DP GC/Ni <sub>2</sub> CoP <sub>2</sub>	6L-3DP GC/Ni <sub>2</sub> CoP <sub>2</sub>
R <sub>s</sub> (Ω cm <sup>2</sup> )	2.82	3.68	4.65
R <sub>ct</sub> (Ω cm <sup>2</sup> )	0.42	0.57	0.69

**Table S3.** Comparison of UOR performance of 3DP GC/Ni<sub>2</sub>CoP<sub>2</sub> with Ni, Co-based electrocatalysts. (*j*: current density; E: potential)

Catalysts	<i>j</i> (mA cm <sup>-2</sup> )	E (V)	Reference
a-MoS <sub>2</sub> /CoS/Co <sub>0.85</sub> Se HNTs	50	1.38	<i>Nanoscale</i> , 2020, <b>12</b> , 991
Ni <sub>2</sub> P/Fe <sub>2</sub> P/NF	10	1.36	<i>J. Colloid Interf. Sci.</i> , 2019, <b>541</b> , 279-286
Co-Ni-S@NF	10	1.31	<i>J. Mater. Chem. A</i> , 2022, <b>10</b> , 24137
Co-V-NiS <sub>2</sub>	10	1.35	<i>ACS Catal.</i> , 2022, <b>12</b> , 569-579
Co-NiMoO <sub>4</sub> -Ar	10	1.324	<i>J. Mater. Chem. A</i> , 2022, <b>10</b> , 16825
Ni(OH)S/NF	10	1.34	<i>Appl. Catal. B Environ.</i> , 2022, <b>312</b> , 121389
NC-FNCP	10	1.37	<i>Nano Res.</i> , 2022, <b>15</b> , 1916-1925
CoNi LDH	10	1.32	<i>ACS Appl. Mater. Interfaces</i> , 2022, <b>14</b> , 16222-16232
Ni <sub>3</sub> S <sub>2</sub> /NF	10	1.34	<i>ACS Appl. Mater. Interfaces</i> , 2021, <b>13</b> , 35709-35718
<b>3DP GC/Ni<sub>2</sub>CoP<sub>2</sub></b>	<b>10</b>	<b>1.31</b>	<b>This work</b>

**Table S4** Comparison of HER performance of 3DP GC/Ni<sub>2</sub>CoP<sub>2</sub> with Ni, Co-based electrocatalysts. (*j*: current density;  $\eta$ : overpotential)

Catalysts	<i>j</i> (mA cm <sup>-2</sup> )	$\eta$ (mV)	Reference
a-MoS <sub>2</sub> /CoS/Co <sub>0.85</sub> Se HNTs	10	127	<i>Nanoscale</i> , 2020, <b>12</b> , 991
Ni <sub>2</sub> P/Fe <sub>2</sub> P/NF	10	115	<i>J. Colloid Interf. Sci.</i> , 2019, <b>541</b> , 279-286
Ni-Co-P HNBs	10	107	<i>Energy Environ. Sci.</i> , 2018, <b>11</b> , 872
Fe-CoP HTPAs	10	98	<i>Small</i> , 2018, <b>14</b> , 1704233
NiCoP/NF	10	95	<i>J Mater. Chem. A</i> , 2023, <b>11</b> , 1256
NiCoP-90	10	93	<i>Adv. Energy Mater.</i> , 2023, <b>12</b> , 2300499
Ni <sub>0.2</sub> S/Cu <sub>5</sub> FeS <sub>4</sub>	10	140	<i>J. Colloid Interf. Sci.</i> , 2020, <b>578</b> , 668-676
r-NiS/h-NiS	10	101	<i>J. Colloid Interf. Sci.</i> , 2023, <b>633</b> , 640-648
Ni NDs <sub>45</sub>	10	204	<i>Mol. Catal.</i> , 2021, <b>516</b> , 112006
Co <sub>0.9</sub> Ni <sub>0.1</sub> Se with vacancies	10	185.7	<i>Mol. Catal.</i> , 2022, <b>525</b> , 112339
Ni-SA/NC	10	102	<i>Angew. Chem. Int. Ed.</i> , 2020, <b>59</b> , 22743-22748
NiCo <sub>2</sub> -P	10	183	<i>Adv. Mater.</i> , 2020, <b>33</b> , 2003846
HC NiCo/C	10	99	<i>ACS Appl. Mater. Interfaces</i> , 2021, <b>13</b> , 9932-9941
NiCo DASs/N-C	10	189	<i>Adv. Funct. Mater.</i> , 2023, <b>33</b> , 2210867
NiCoO-NiCo/C	10	123	<i>Appl. Catal. B Environ.</i> , 2021, <b>292</b> , 120170
3DP GC/Ni <sub>2</sub> CoP <sub>2</sub>	10	95.6	This work

**Video S1.** Electrolyte transmission behaviour of 3DP GC electrode.

**Video S2.** Electrolyte transmission behaviour of CP electrode.